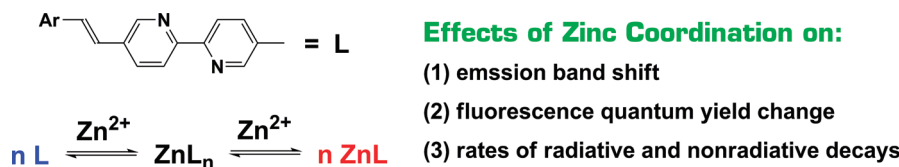# Fluorescence of 5-Arylvinyl-5′-Methyl-2,2′-Bipyridyl Ligands and Their Zinc Complexes

Ali H. Younes, Lu Zhang, Ronald J. Clark, and Lei Zhu*

Department of Chemistry and Biochemistry, Florida State University, Tallahassee, Florida 32306-4390

lzhu@chem.fsu.edu

Received September 1, 2009

Effects of Zinc Coordination on:

(1) emssion band shift

(2) fluorescence quantum yield change

(3) rates of radiative and nonradiative decays

The photophysical properties of 5-arylvinyl-5′-methyl-2,2′-bipyridyls (AVMBs, **1**−**9**, **11**) and their zinc complexes were studied. Similar 2,2′-bipyridyl-based ligands have been applied as optical sensors for metal ions and sensitizers for solar energy conversion. The goal of this investigation is to reveal the factors that determine the emission band shift and fluorescence quantum yield change of the title ligand system upon zinc binding. The outcome of this study will not only advance the fundamental understanding of the coordination-driven photophysical processes embodied in the AVMB platform but facilitate the rational design of fluorescent probes for metal ions, particularly zinc. The AVMB ligands were synthesized using the Horner−Wadsworth−Emmons reaction. AVMBs containing electron-donating aryl groups show absorption and emission in the visible region, which can be assigned to charge-transfer transitions as supported by solvent-dependency and computational studies. The binding between AVMB ligands and zinc ion in acetonitrile was studied using isothermal titration calorimetry (ITC). A multicomponent equilibrium model is suggested that explains the multiple transitions evidenced in fluorescence titration isotherms. Coordination to zinc ion stabilizes the charge-transfer excited state of an AVMB ligand with an electron-donating aryl substituent, consequently results in bathochromic shifts in both absorption and emission. However, unlike the emission band shift, the fluorescence quantum yield change upon zinc complex formation does not have an intuitive correlation with the electronic nature of the aryl group. Lifetime measurements using the Time-Correlated Single Photon Counting method enabled the determination of nonradiative and radiative decay rate constants. Both rates of an AVMB ligand decrease upon zinc binding. The collective effect gives rise to the change in fluorescence quantum yield with the apparent lack of correlation with the electronic property of the aryl group.

Introduction

Conjugated donor−acceptor type chromophores have been investigated to satisfy fundamental and practical interests.[1−13]

Aryl-substituted 2,2′-bipyridyl, 2,2′:6′,2″-terpyridyl, and 1,10-phenanthrolyl donor−acceptor systems possess an extra dimension to their optical properties because metal coordination significantly alters the photophysical processes that they are

(1) Slama-Schwok, A.; Blanchard-Desce, M.; Lehn, J.-M. *J. Phys. Chem.* **1990**, *94*, 3894–3902.

(2) Anstead, G. M.; Garlson, K. E.; Kym, P. R.; Hwang, K.-J.; Katzenellenbogen, J. A. *Photochem. Photobiol.* **1993**, *58*, 785–794.

(3) Meier, H.; Gerold, J.; Kolshorn, H.; Mühling, B. *Chem.—Eur. J.* **2004**, *10*, 360–370.

(4) Meier, H. *Angew. Chem., Int. Ed.* **2005**, *44*, 2482–2506.

(5) Marsden, J. A.; Miller, J. J.; Shirtcliff, L. D.; Haley, M. M. *J. Am. Chem. Soc.* **2005**, *127*, 2464–2476.

(6) Yamaguchi, Y.; Tanaka, T.; Kobayashi, S.; Wakamiya, T.; Matsubara, Y.; Yoshida, Z.-i. *J. Am. Chem. Soc.* **2005**, *127*, 9332–9333.

(7) Butler, R. S.; Myers, A. K.; Bellarmine, P.; Abboud, K. A.; Castellano, R. K. *J. Mater. Chem.* **2007**, *17*, 1863–1865.

(8) Singh, T. S.; Mitra, S.; Chandra, A. K.; Tamai, N.; Kar, S. *J. Photochem. Photobiol. A.* **2008**, *197*, 295–305.

(9) Yamaguchi, Y.; Shimoi, Y.; Ochi, T.; Wakamiya, T.; Matsubara, Y.; Yoshida, Z.-i. *J. Phys. Chem. A* **2008**, *112*, 5074–5084.

(10) Würthner, F.; Archetti, G.; Schmidt, R.; Kuball, H.-G. *Angew. Chem., Int. Ed.* **2008**, *47*, 4529–4532.

(11) Jarowski, P. D.; Wu, Y.-L.; Schweizer, W. B.; Diederich, F. *Org. Lett.* **2008**, *10*, 3347–3350.

capable of.[14−24] In most cases, metal coordination enhances the charge-transfer character of the excited state of the chromophore, provided that the 2,2′-bipyridyl metal chelating site is also the electron acceptor in the metal-free form. The studies of one particular class of the aryl-substituted 2,2′-bipyridyls, the fluorescent arylvinyl-2,2′-bipyridyl (arylvinyl-bipy) ligands, have been intensified in recent years. Their intriguing metal coordination-driven photophysical properties have enabled applications including the development of nonlinear optical materials,[18,25−28] sensitizers for solar cells,[29,30] and metal ion sensors.[14,17,22,31−33]

Our interest in fluorescent arylvinyl-bipy ligands arises from their incorporation into a heteroditopic ligand framework (Figure 1A) for quantifying Zn^{2+} concentration ([Zn(II)]) over large ranges.[34,35] The 5- and/or 5′-aryl-substituted 2,2′-bipyridyls (bipy), which include the fluorophores in our ditopic ligands, are known to possess particularly high fluorescence quantum yields comparing to other substituted bipy derivatives.[15,16] The *ditopic* ligand, however, is designed to be largely nonfluorescent due to the photoinduced electron transfer (PET) from the electron-donating high-affinity Zn^{2+} binding site (dipicolylamino site as shown in Figure 1A) to the excited arylvinyl-bipy fluorophore. The preferential binding of Zn^{2+} at the dipicolylamino site decreases the oxidation potential of the electron-donating tertiary amino group. Consequently, the thermodynamic driving force of PET is diminished to result in a chelation-enhanced fluorescence (CHEF). When [Zn(II)] is adequately high, the bipy site is also coordinated. The presumed charge-transfer excited state of arylvinyl-bipy

(A)

OFF   BLUE   RED

CHEF   ICT

(B)
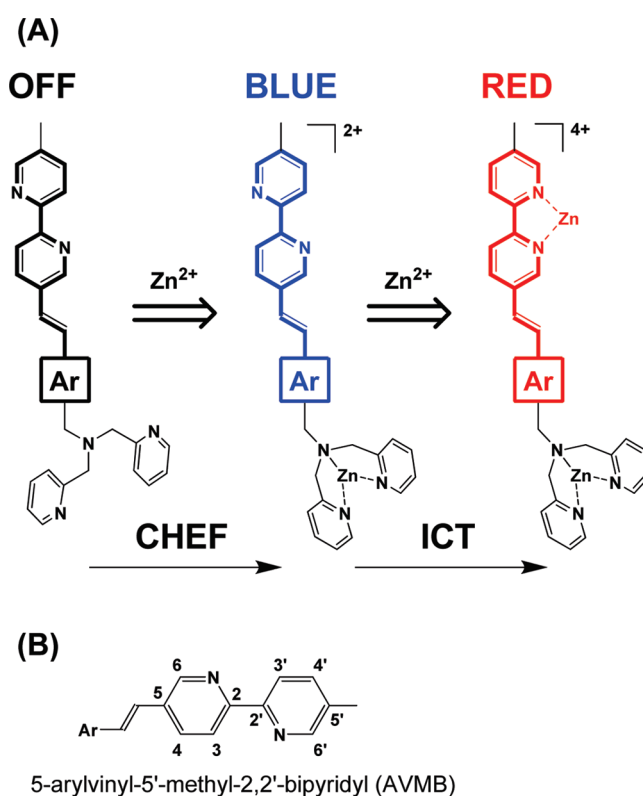
5-arylvinyl-5'-methyl-2,2'-bipyridyl (AVMB)

FIGURE 1. (A) Fluorescent heteroditopic ligand platform contains a 5-arylvinyl-2,2′-bipyridyl fluoroionophore (bold). CHEF, chelation-enhanced fluorescence; ICT, internal (or intramolecular) charge transfer. The blue and red colors represent two different emission wavelengths (short and long). They do not correspond to the true color ranges of blue and red. (B) Structure and numbering scheme of the title ligand system (AVMB) in this article.

is consequently stabilized to lead to an emission bathochromic shift. The relative abundance of the three fluorescence states (OFF, BLUE, and RED) of a ditopic ligand is dependent upon [Zn(II)]. By relating the fluorescence intensity at the BLUE and RED channels to [Zn(II)], the quantification of [Zn(II)] over a relatively broad range can be achieved.

Important factors that determine the sensitivity of [Zn(II)] quantification using our heteroditopic system include (1) the extent of CHEF upon Zn^{2+} binding at the dipicolylamino group, (2) the magnitude of shift that the emission band of the AVMB fluorophore undergoes (i.e., from BLUE to RED in Figure 1A) upon Zn^{2+} coordination at the bipy site, and (3) the fluorescence quantum yields of the mono- and dicoordinated complexes. The first factor is related to the oxidation potential of the fluorophore. A fluorophore with a low oxidation potential would afford a large thermodynamic driving force of PET from the dipicolylamino donor group to the excited fluorophore in the free ditopic ligand shown in Figure 1A, which amplifies the CHEF effect when Zn^{2+} is coordinated.[35] For factor #2, larger emission band shift would result in smaller overlap between BLUE and RED channels, which would lead to better sensitivity. In this article, we primarily describe the studies on the factors (#2 and #3) that determine the extent of emission band shift and fluorescence quantum yield change of AVMB fluorophores (Figure 1B) upon Zn^{2+} coordination. In addition to aiding the rational designs of fluorescent probes for metal ions that

(12) Boydston, A. J.; Vu, P. D.; Dykhno, O. L.; Chang, V.; Wyatt, A. R. I.; Stockett, A. S.; Ritschdorff, E. T.; Shear, J. B.; Bielawski, C. W. *J. Am. Chem. Soc.* **2008**, *130*, 3143–3156.

(13) Butler, R. S.; Cohn, P.; Tenzel, P.; Abboud, K. A.; Castellano, R. K. *J. Am. Chem. Soc.* **2009**, *131*, 623–633.

(14) Wang, B.; Wasielewski, M. R. *J. Am. Chem. Soc.* **1997**, *119*, 12–21.

(15) Joshi, H. S.; Jamshidi, R.; Tor, Y. *Angew. Chem., Int. Ed.* **1999**, *38*, 2722–2725.

(16) Loren, J. C.; Siegel, J. S. *Angew. Chem., Int. Ed.* **2000**, *40*, 754–757.

(17) Leroy, S.; Soujanya, T.; Fages, F. *Tetrahedron Lett.* **2001**, *42*, 1665–1667.

(18) Maury, O.; Guegan, J.-P.; Renouard, T.; Hilton, A.; Dupau, P.; Sandon, N.; Toupet, L.; Le Bozec, H. *New J. Chem.* **2001**, *25*, 1553–1566.

(19) Wang, X.-y.; Guerzo, A. D.; Schmehl, R. H. *Chem. Commun.* **2002**, 2344–2345.

(20) Vaidya, S.; Johnson, C.; Wang, X.-Y.; Schmehl, R. H. *J. Photochem. Photobiol. A.* **2007**, *187*, 258–262.

(21) Mutai, T.; Araki, K. *Curr. Org. Chem.* **2007**, *11*, 195–211.

(22) Leroy-Lhez, S.; Allain, M.; Oberle, J.; Fages, F. *New J. Chem.* **2007**, *31*, 1013–1021.

(23) Sun, Y.; Ross, N.; Zhao, S.-B.; Huszarik, K.; Jia, W.-L.; Wang, R.-Y.; Macartney, D.; Wang, S. *J. Am. Chem. Soc.* **2007**, *129*, 7510–7511.

(24) Sun, Y.; Wang, S. *Inorg. Chem.* **2009**, *48*, 3755–3767.

(25) Dhenaut, C.; Ledoux, I.; Samuel, I. D. W.; Zyss, J.; Bourgault, M.; Le Bozec, H. *Nature* **1995**, *374*, 339–342.

(26) Bourgault, M.; Baum, K.; Le Bozec, H.; Pucetti, G.; Ledoux, I.; Zyss, J. *New J. Chem.* **1998**, 517–522.

(27) Renouard, T.; Le Bozec, H.; Brasselet, S.; Ledoux, I.; Zyss, J. *Chem. Commun.* **1999**, 871–872.

(28) Senechal, K.; Maury, O.; Le Bozec, H.; Ledoux, I.; Zyss, J. *J. Am. Chem. Soc.* **2002**, *124*, 4560–4561.

(29) Wang, P.; Klein, C.; Humphry-Baker, R.; Zakeeruddin, S. M.; Gratzel, M. *J. Am. Chem. Soc.* **2005**, *127*, 808–809.

(30) Jang, S.-R.; Lee, C.; Choi, H.; Ko, J. J.; Lee, J.; Vittal, R.; Kim, K.-J. *Chem. Mater.* **2006**, *18*, 5604–5608.

(31) Chen, L. X.; Jager, W. J. H.; Gosztola, D. J.; Niemczyk, M. P.; Wasielewski, M. R. *J. Phys. Chem. B* **1997**, *104*, 1950–1960.
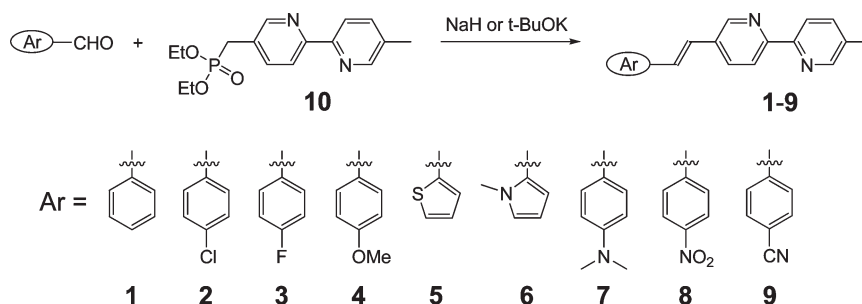
(32) Ajayaghosh, A.; Carol, P.; Sreejith, S. *J. Am. Chem. Soc.* **2005**, *127*, 14962–14963.

(33) Dennis, A. E.; Smith, R. C. *Chem. Commun.* **2007**, 4641–4643.

(34) Zhang, L.; Clark, R. J.; Zhu, L. *Chem.—Eur. J.* **2008**, *14*, 2894–2903.

(35) Zhang, L.; Zhu, L. *J. Org. Chem.* **2008**, *73*, 8321–8330.

SCHEME 1

are effective over large concentration ranges[34,36] and molecular logic functions,[37] the conclusion of this study is expected to advance our understanding of fundamental coordination-driven photophysical processes embodied in this class of fluorescent compounds.

Results and Discussion

Synthesis. Compounds **1**−**9** were prepared via Horner−Wadsworth−Emmons reactions using, in most cases, NaH as the base between various arylaldehydes and phosphonate **10** (Scheme 1). When arylaldehydes with electron-withdrawing substituents were used (**3**, **8**, and **9**), *t*-BuOK which is unable to reduce the arylaldehydes, was employed as the base instead. All of the products were isolated as trans isomers after purification using silica gel chromatography in good yields (70−80%). Some of the products were further purified via recrystallization in either dichloromethane (DCM) or ethyl acetate (EtOAc).

Compound **11** was prepared by direct bromination of **6** with Br$_2$ (Scheme 2). The electron-rich *N*-methylpyrrole ring

SCHEME 2
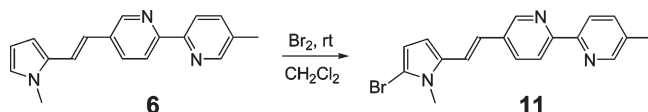
was brominated selectively over the alkene in **6**. The 1-bromo-*N*-methylpyrrole group with strengthened electron-withdrawing ability slows down the dibromination of the alkene which allowed the isolation of **11** in 48%.

X-Ray Crystal Structure of 6. The single crystals of compound **6** were grown via slow evaporation of a solution of **6** in a mixture of hexanes and DCM. In addition to a transoid conformation in the 2,2′-bipy unit,[38] only one conformer in respect to the rotations of the C1−C2 and C3−C4 bonds was observed (Figure 2A). The dipole moments of neighboring aromatic rings are aligned opposite each other to minimize the overall dipole moment of the molecule. In contrast to the bipy-containing structures without arylvinyl caps which show 6−7° (or larger) dihedral

angles between the two pyridyl rings,[34,39−41] the bipy moiety in **6** is completely planar along with the double bond (Figure 2B). The *N*-methylpyrrole group has a slight twist off the plane of the vinyl-bipy moiety to minimize the steric
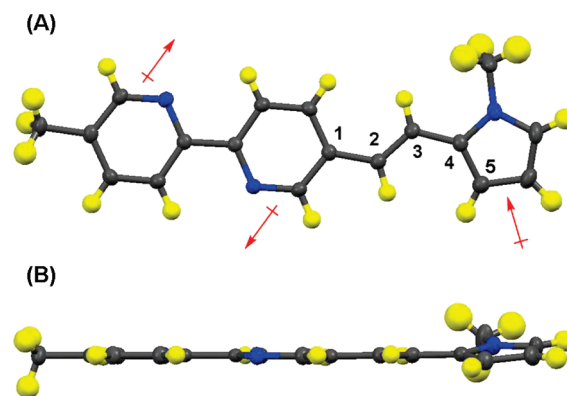
FIGURE 2. Two views of the X-ray crystal structure of **6** (50% probability ellipsoids). Black, carbon; blue, nitrogen; yellow, hydrogen. The dipole moment vectors of the individual aromatic rings in **6** are shown in (A).

congestion between the *N*-methyl group and the vinyl hydrogen. The dihedral angle (C2−C3−C4−C5) is 12.11°.

Cyclic Voltammetry Studies. The motivation for the cyclic voltammetry studies was to determine the HOMO energy levels (which are related to the oxidation potentials) of the AVMB ligands so that the relative efficiency of PET in the heteroditopic framework shown in Figure 1 can be predicted. All the ligands undergo irreversible electrochemical oxidation as shown in their cyclic voltammograms (Supporting Information, SI). The first anodic peak potentials are listed in Table 1. The increased electron-donating ability of an aryl group results in a higher oxidation potential (or oxidizability). As shown in a previous study,[35] the heteroditopic ligand containing **1** (E_{pa} = 1.57 V vs Ag/AgCl) as the fluorophore demonstrates high efficiency of PET, whereas the incorporation of the electron-richer ligand **5** (E_{pa} = 1.36 V) results in much lower PET efficiency. Based on the E_{pa} data shown in Table 1, compounds **2**, **3**, **8**, and **9** which have larger anodic peak potentials (lower oxidation potentials) than that of **1** are expected to be efficient electron-acceptors when excited in the heteroditopic framework. Consequently, a sensitive CHEF of the ditopic ligand may

(36) Zhu, L.; Zhang, L.; Younes, A. H. *Supramol. Chem.* **2009**, *21*, 268−283.

(37) Zhang, L.; Whitfield, W. A.; Zhu, L. *Chem. Commun.* **2008**, 1880−1882.
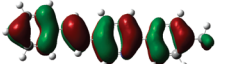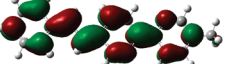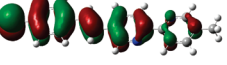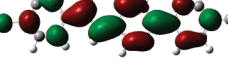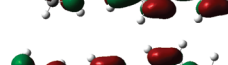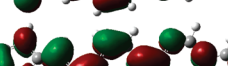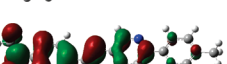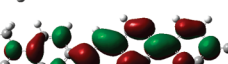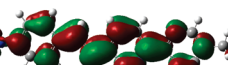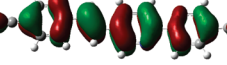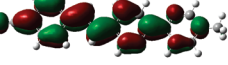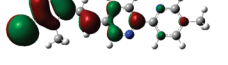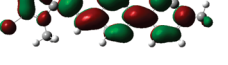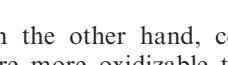
(38) Zahn, S.; Reckien, W.; Kirchner, B.; Staats, H.; Matthey, J.; Lützen, A. *Chem.—Eur. J.* **2009**, *15*, 2572−2580.

(39) Newkome, G. R.; Nayak, A.; Fronczek, F.; Kawato, T.; Taylor, H. C. R.; Meade, L.; Mattice, W. *J. Am. Chem. Soc.* **1979**, *101*, 4472−4477.

(40) Hanan, G. S.; Lehn, J.-M.; Kyritsakas, N.; Fischer, J. *J. Chem. Soc., Chem. Commun.* **1995**, 765−766.

(41) Jouvenot, D.; Glazer, E. C.; Tor, Y. *Org. Lett.* **2006**, *8*, 1987−1990.

TABLE 1. Computed HOMO and LUMO Molecular Orbitals at the B3LYP/6-31++G(d,p) level, and the First Anodic Peak Potentials (vs Ag/AgCl) with the Calculated HOMO−LUMO Gap of 1−9 and 11

ligand	HOMO	LUMO	E_{pa}/V (HOMO-LUMO gap/nm)
1			1.57 (337)
2			1.65 (343)
3			1.57 (340)
4			1.29 (354)
5			1.36 (356)
6			0.78 (367)
7			0.64 (382)
8			2.10 (364)
9			1.89 (356)
11			0.51 (368)

occur when Zn^{2+} is present. On the other hand, compounds **4**, **6**, **7**, and **11** which are more oxidizable than **4** might not perform well with dipicolylamino group as a PET pair.[42]

Computational Studies. The frontier molecular orbitals of all the AVMBs were computed at the B3LYP/6-31++G(d,p) level. For AVMBs with electron-donating aryl groups (**4**, **5**, **6**, **7**, and **11**), and to a lesser extent compounds **2** and **3**, the electron density of each molecule shows a net shift from the aryl side of the highest occupied molecular orbital (HOMO) to the pyridyl side of the lowest unoccupied molecular orbital (LUMO, Table 1), which is consistent with a charge-transfer transition to the S_1 state. Although the chloro (**2**) and the fluoro (**3**) substituents are electron-withdrawing, they are considered to be electron donors through resonance. Therefore, charge-transfer from the aryl moiety to the pyridyl side is also expected for **2** and **3** upon excitation. Intramolecular charge transfer in **8** and **9**, if there is any, appears to occur in the opposite direction to the nitro and cyano substituents, respectively. The electron density resides on the bond

connecting the nitro or the cyano substituent and the aryl ring in the LUMOs of **8** and **9** appears to be higher than those in other ligands.

The structure-dependent trend of the calculated HOMO/LUMO gaps (in nanometers, Table 1) correlates well with the trend of the experimentally determined wavelengths at maximum absorption (λ_{max} in Table 3). It appears that the electron density of the aryl group in an AVMB determines the extent of charge transfer in its excited state, the oxidizability (E_{pa}), and the HOMO/LUMO gap (or λ_{max} of absorption) of the compound. The enhancement of the electron-donating ability of the aryl group leads to more pronounced charge-transfer in the excited state, a greater oxidizability, and a smaller HOMO/LUMO gap (which results in a bathochromic shift in absorption).[43] This correlation may be unique in chromophores capable of internal charge transfer (ICT), which may pose a dilemma in engineering fluorescent heteroditopic ligands with large contrast between the three fluorescence states shown in Figure 1A.

(42) Ueno, T.; Urano, Y.; Setsukinai, K.-i.; Takakusa, H.; Kojima, H.; Kikuchi, K.; Ohkubo, K.; Fukuzumi, S.; Nagano, T. *J. Am. Chem. Soc.* **2004**, *126*, 14079–14085.

(43) Anslyn, E. V.; Dougherty, D. A. In *Modern Physical Organic Chemistry*; University Science Books: Sausalito, CA, 2006; Chapter 3, p 186.

TABLE 2. Photophysical Parameters of 6 and its Zn²⁺ Complex in Various Solvents[a]

	HX	BZ	DX	TL	CHCl₃	EtOH	MeOH	MeCN	DMF	DMSO
ε	2.02	2.3	2.3	2.4	4.8	25	33	36.6	38.3	47
λ_{abs}/nm	372	382	381	382	380	383	382	378	384	388
λ_{em}/nm	436	464	464	459	476	501	507	488	493	500
SS/cm⁻¹	3946	4626	4695	4392	5307	6150	6454	5963	5758	5773
ϕ_f	0.36	0.24	0.24	0.25	0.25	0.20	0.18	0.087	0.19	0.19
τ/ns	0.86	0.51	0.59	0.56	0.62	0.92	1.00	0.51	0.65	0.64
χ^2	0.42	0.60	0.56	0.40	0.95	0.69	0.85	0.47	0.70	0.72
k_r/ns⁻¹	0.42	0.46	0.41	0.44	0.40	0.22	0.18	0.17	0.28	0.30
k_{nr}/ns⁻¹	0.75	1.50	1.29	1.34	1.22	0.86	0.82	1.79	1.25	1.26
λ_{abs}/nm (Zn²⁺ complex)	ND[d]	ND[d]	428[b]	ND[d]	447[c]	426	426	421	419	423
λ_{em}/nm (Zn²⁺ complex)	ND[d]	ND[d]	587[b]	ND[d]	583[c]	589	586	607	587	585

[a]Abbreviations: HX, hexanes; BZ, benzene; DX, dioxane; TL, toluene; CHCl₃, chloroform; EtOH, ethanol; MeOH, methanol; MeCN, acetonitrile; DMF, dimethylformamide; DMSO, dimethylsulfoxide; ε, relative permittivity of a solvent; SS, Stokes Shift; τ, lifetime; χ^2, reduced goodness-of-fit parameter; k_r, radiative decay rate constant; k_{nr}: non-radiative decay rate constant. [b]Data were collected in THF. Compound **6** shows incomplete coordination with Zn²⁺ in dioxane. [c]Data were collected in DCM. Compound **6** shows incomplete coordination with Zn²⁺ in CHCl₃. [d]ND, Not Determined.
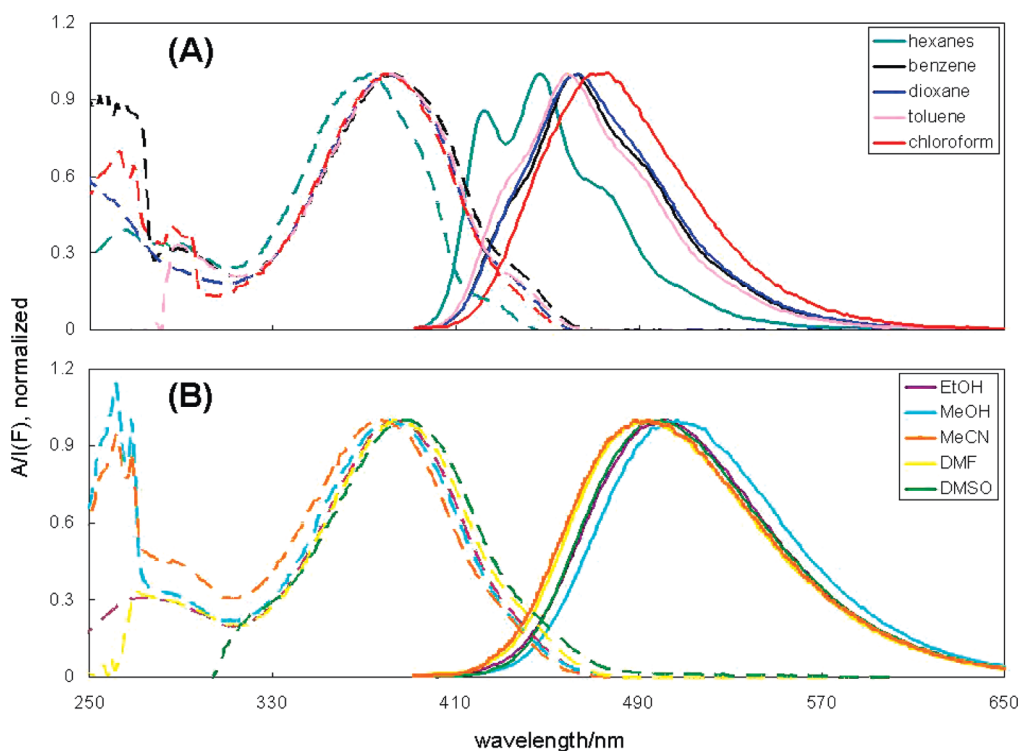
FIGURE 3. Normalized absorption (dashed lines) and emission (solid lines) spectra of **6** in different solvents. (A) Spectra collected in "nonpolar" solvents; (B) spectra collected in "polar" solvents.

Solvent Dependency Studies. 1. Solvent Effect on Absorption Spectra. The absorption spectra of compound **6**, which was selected as an example of AVMBs containing electron-donating aryl groups, were collected in solvents (Figure 3, dashed lines) of different polarities and hydrogen bond donating abilities. Two absorption bands of high molar absorptivities were observed at ∼260 and ∼380 nm, respectively. Both bands are rather insensitive to solvent except in hexanes where the band of the lowest energy centered at 372 nm and is relatively structured. The wavelengths at maximal absorption and related molar absorptivities as well as other photophysical parameters are listed in Table 2.

2. Solvent Effect on Emission Spectra. The emission spectra of **6** are shown in Figure 3 (solid lines). The positive

solvatofluorochromism[12] is evident which suggests the formation of an emissive polar excited state.[44] The spectrum in hexanes is clearly structured with vibronic bands. As solvent polarity increases, the emission band gradually loses its vibronic structure to become rounded, which can be assigned to the emission from a charge-transfer excited state. The hydrogen bond donating solvents such as MeOH ($\varepsilon = 33$) and EtOH ($\varepsilon = 25$) enable larger emission bathochromic shifts (from hexanes) than polar aprotic solvents such as DMSO ($\varepsilon = 47$). The specific solvent effect shown in MeOH and EtOH can be attributed to the strengthened hydrogen bond between the solvent molecule and the charge-transfer excited state (Figure 4).[45] The solvent effect on the emission of **6** (and **7** in SI) is similar to what was observed in the

(44) Suppan, P.; Ghoneim, N. *Solvatochromism*; The Royal Society of Chemistry: London, 1997.

(45) Lakowicz, J. R. In *Principles of Fluorescence Spectroscopy*, 3rd ed.; Springer: New York, 2006; Chapter 7.
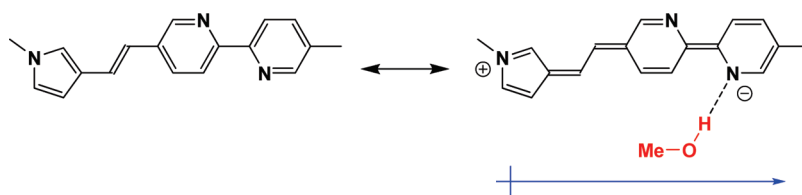
FIGURE 4. Schematic representation of hydrogen bonding between MeOH and excited **6** (the charge-separated resonance structure).[36]

dimethylaminostyryl terpyridine derivative reported by Schmehl et al.[20]

The magnitude of solvatofluorochromism is related to the electron-donating ability of the aryl substituent. The electron-deficient 4-cyanophenyl group enables very little solvent-induced spectral shift of **9** (Figure S10, SI) whereas compound **7** containing a more electron-donating 4-dimethylaminophenyl group shows more sensitive solvent effect (Figure S9, SI) than that of **6**. The Stokes shifts of **6** and **7** were plotted against the orientation polarizabilities of the solvents to afford the Lippert plots (Figure 5).[45] The radius of the cavity (a) where the fluorophore resides is assumed to be similar in all solvents so that the slope of the plot represents the degree of polarization upon excitation based on the Lippert-Magata equation (eq 1). The linearity of both plots is only moderate due to the presence of (1) transitions of different natures (i.e., locally excited and charge-transfer), and (2) specific solvent effects, which are not considered in the theoretical model for the Lippert-Magata equation. Specifically, the relatively structured emission spectra collected in nonpolar solvents, in particular hexanes (Figure 3A, solid lines), and the smooth spectra obtained in polar solvents (Figure 3B, solid lines) are likely originated from different emissive states. In EtOH and MeOH, the hydrogen bond donating ability (not represented by the orientation polarizability) in addition to their general polarity determines the magnitude of the Stokes shift. The qualitative conclusion drawn from the Lippert plots is that ligand **7** which contains a more electron-donating aryl group undergoes a higher degree of polarization upon photoexcitation than that of **6**.

$$\text{Stokes Shift(SS)} = \nu_A - \nu_F = \frac{2\Delta f}{\hbar c a^3}(\mu_E - \mu_G)^2 + \text{const} \quad (1)$$

ν_A, absorption in wavenumber; ν_F, emission in wavenumber; $\hbar$, Planck's constant; c, speed of light; a, radius of the cavity in which the fluorophore resides; μ_E, excited state dipole; μ_G, ground state dipole.

$$\Delta f = \frac{\varepsilon - 1}{2\varepsilon + 1} - \frac{n^2 - 1}{2n^2 + 1} \quad (2)$$

ε, relative permittivity or dielectric constant of a solvent; n, refractive index.

3. Solvent Effect on Lifetimes and Fluorescence Quantum Yields. Lifetimes (τ) of **6** (Table 2) were determined using the time-correlated single photon counting (TCSPC) method. In a TCSPC experiment, the detector is adjusted to capture only a single photon emitted by the sample after each excitation pulse. This photon is recorded in a time channel correlated to the time lapse between the excitation and the detection. After repetitive pulsed excitations, the numbers of photons collected in all the channels are used to reconstruct the
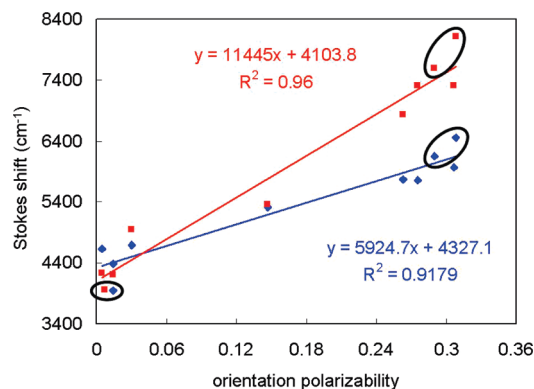

FIGURE 5. Lippert plots of compounds **6** (blue) and **7** (red). Data derived from hexanes are grouped in the circle on the left, and the data derived from EtOH and MeOH are grouped in the two circles on the right. Equation 2 was used to calculate the orientation polarizability.

fluorescence intensity decay curve from which the lifetime value(s) can be extracted.[46,47] As evidenced by the small reduced χ^2 values, single exponentials were adequate to fit the fluorescence decay traces collected in various solvents.[48] Combining with the fluorescence quantum yield (ϕ_f) of **6**, which was found to decrease slightly with increasing solvent polarity, the radiative and nonradiative decay rates (k_r and k_{nr}, Table 2) were calculated using eqs 3 and 4.

The lifetimes of **6** in all solvents are short (< 1 ns). Similarly solvent-dependent short lifetimes have been reported for ICT-type compounds such as 4-methylamino-4'-cyanostilbene[49] and N-alkyl-4-(p-N,N-dimethylaminostyryl)pyridinium bromide.[50] Relatively large values were recorded in hydrogen bonding solvents (0.92 ns in EtOH and 1.0 ns in MeOH). The radiative rate constant (k_r) decreases with increasing solvent polarity (e.g., comparing the rates in solvents listed in Figure 3B vs those in Figure 3A). Such a solvent dependency of k_r can be explained using eq 5 derived by Stricker and Berg, by which a shorter maximum absorption wavelength leads to a larger radiative decay rate.[51,52] In hexanes and two hydrogen bonding solvents, low nonradiative decay rates (k_{nr}) were observed. The low k_{nr} in

(46) Valeur, B. In *Molecular Fluorescence. Principles and Applications*; WILEY-VCH: New York, 2002; pp 173−176.

(47) Lakowicz, J. R. In *Principles of Fluorescence Spectroscopy*, 3rd ed.; Springer: New York, 2006; pp 103−107.

(48) Lakowicz, J. R. In *Principles of Fluorescence Spectroscopy*, 3rd ed.; Springer: New York, 2006; pp 129−133.

(49) Abraham, E.; Oberlé, J.; Jonusauskas, G.; Lapouyade, R.; Rullière, C. *Chem. Phys.* **1997**, *214*, 409–423.

(50) Mishra, A.; Behera, G. B.; Krishna, M. M. G.; Periasamy, N. *J. Lumin.* **2001**, *92*, 175–188.

(51) Montalti, M.; Credi, A.; Prodi, L.; Gandolfi, M. T. In *Handbooks of Photochemistry*, 3rd ed.; CRC Taylor and Francis: London, 2006; pp 25−28.

(52) Turro, N. J.; Ramamurthy, V.; Scaiano, J. C. In *Principles of Molecular Photochemistry, An Introduction*; University Science Books: Sausalito, CA, 2009; pp 195−196.
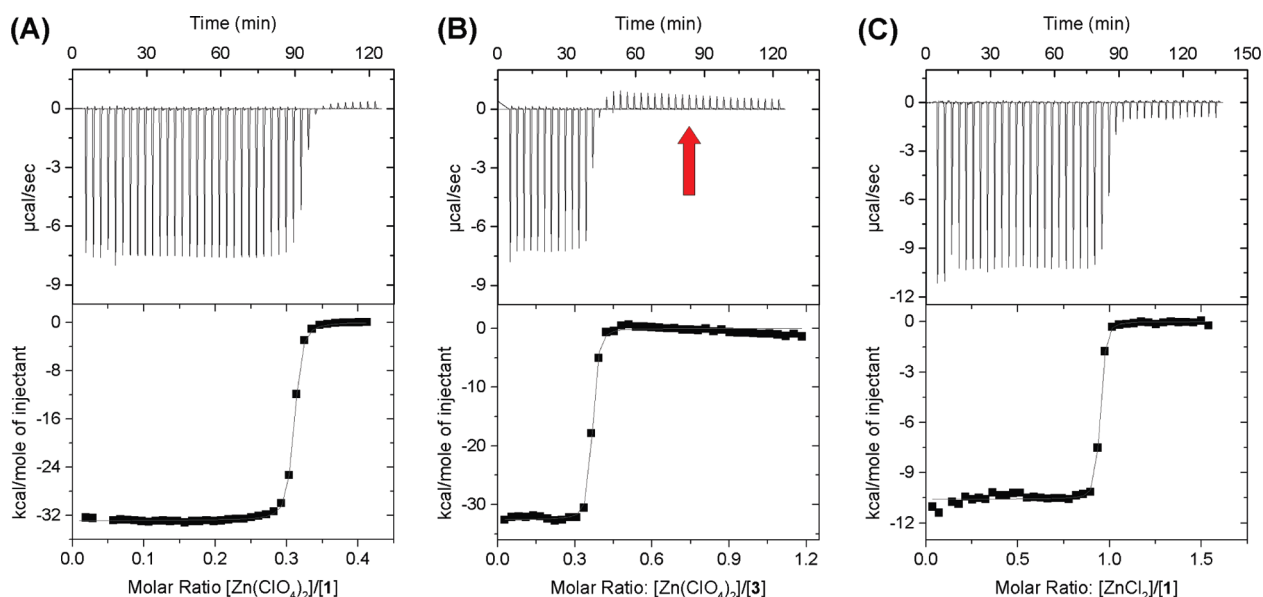
FIGURE 6. ITC titrations of (A) **1** (0.40 mM) with $Zn(ClO_4)_2$ (0.93 mM), n (molar ratio) $= 0.31$, $\Delta H^\circ = -33 \pm 0.05$ kcal/mol, $K = (3.3 \pm 0.16) \times 10^7 \, M^{-1}$, $\Delta S^\circ = -76$ eu; (B) **3** (0.14 mM) with $Zn(ClO_4)_2$ (0.93 mM), $n = 0.35$, $\Delta H^\circ = -33 \pm 0.2$ kcal/mol, $K = (2.6 \pm 0.51) \times 10^7 \, M^{-1}$, $\Delta S^\circ = -75$ eu. The small endothermic transition is marked by the red arrow; (C) **1** (0.40 mM) with $ZnCl_2$ (3.4 mM), $n = 0.93$, $\Delta H^\circ = -11 \pm 0.05$ kcal/mol, $K = (1.9 \pm 0.36) \times 10^7 \, M^{-1}$, $\Delta S^\circ = -2.1$ eu.

hexanes may result from the relatively weak interactions between solvent and the excited solute. In MeOH and EtOH, the hydrogen bonds between the solvent molecules and the pyridyl groups may have restricted the rotation of the C2−C2′ bond of bipy, which results in low k_{nr}. Other than these three solvents, no obvious dependency of k_{nr} on solvent polarity was observed. It should be noted, however, the explanations accounting for the trends of k_{nr} and k_r of compound **6** may not be entirely applicable to other ligands because specific functional groups contained in other structures may open or close related relaxation pathways.

$$\tau = \frac{1}{k_r + k_{nr}} \quad (3)$$

$$\phi_f = \frac{k_r}{k_r + k_{nr}} \quad (4)$$

$$k_r \propto \nu^2 f \quad (5)$$

ν, the wavenumber corresponding to the maximum absorption wavelength; f, oscillator strength (eq 6).

$$f \equiv 4.3 \times 10^{-9} \int \varepsilon d\nu \propto \langle \Psi_1 | \Psi_2 \rangle^2 \quad (6)$$

Oscillator strength (f) is proportional to the experimentally determined molar absorptivity (ε). $\langle \Psi_1 | \Psi_2 \rangle$ is the transition dipole moment.

Isothermal Titration Calorimetry Studies of Zinc Coordination. 1. Exothermicity of Binding. Isothermal titration calorimetry (ITC) was used to determine the binding stoichiometry of AVMBs to Zn^{2+} in MeCN. In our previous study,[35] a 3:1 (ligand to $Zn(ClO_4)_2$) ratio was reported for 5,5′-dimethyl-2,2′-bipyridyl in MeCN. Herein, the fluorescent analogs **1** and **3** also show a binding stoichiometry of 3:1 (ligand to $Zn(ClO_4)_2$, Figure 6A and B). However, a second, small endothermic transition was also observed (Figure 6B,

indicated by a red arrow) which was tentatively ascribed to the conversion of the 3:1 complex (L_3Zn) to the 2:1 and/or 1:1 complexes (L_2Zn, LZn) at elevated [Zn(II)]. Based on the ITC data, we postulate that the formation of the 3:1 complex is strongly exothermic due to the net gain of the pyridyl-Zn^{2+} dative bonds (Scheme 3). However, the conversion from the 3:1 to 2:1 and/or 1:1 complex at high [Zn(II)] is not as thermally sensitive because only exchanges but no net gain of pyridyl-Zn^{2+} dative bonds are involved (Scheme 4). In the case of ligand **3**, a weakly endothermic transition was observed (Figure 6B).

SCHEME 3
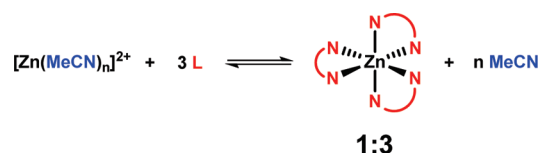
SCHEME 4
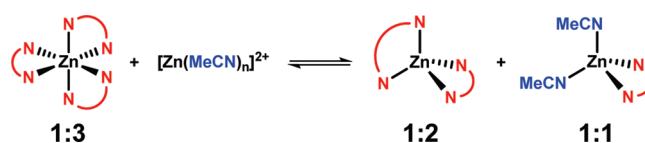
2. Counter Ion Effect on Binding Stoichiometry. The binding stoichiometry of AVMBs with Zn^{2+} salts in MeCN shows a sensitive dependence on counterion. As the more strongly coordinating chloride replaces perchlorate as the counterion, the binding stoichiometry of ligand **1** to Zn^{2+} switches to 1:1 (Figure 6C, Scheme 5). The counterion dependence of binding stoichiometry between Zn^{2+} and the bipy moiety in solution is echoed by the X-ray crystal structures obtained under different conditions. In most
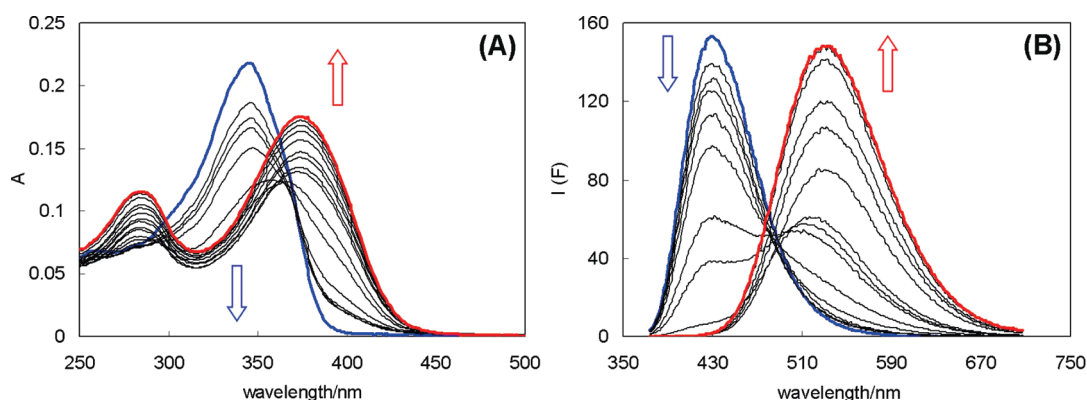
FIGURE 7. (A) Absorption spectra of **4** (6.0 μM) in MeCN upon addition of Zn(ClO$_4$)$_2$ (0−110 μM). (B) Fluorescence spectra of **4** (λ_{ex} = 362 nm, 6.0 μM) in MeCN upon addition of Zn(ClO$_4$)$_2$ (0−26 μM). Blue, spectra of the free ligand; red, spectra at the end of the titration, presumably of the 1:1 complex.

cases, octahedral coordinated Zn^{2+} involving three biden-tate ligands were observed.[53−56] However, when ZnCl$_2$ was used as the Zn^{2+} source, the X-ray crystal structures of the

SCHEME 5
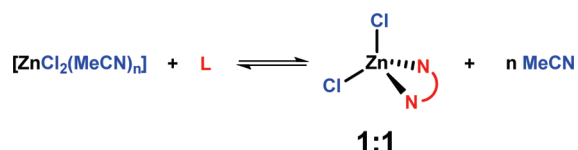
1:1 complexes were obtained by Kozhevnikov et al.[57,58] where Zn^{2+} adopts a tetrahedral geometry with two chloride ions coordinated.

TABLE 3. Position (λ_{max}) and Molar Absorptivities (ε) of the Lowest Energy Absorption Bands of Both Free Ligands and Their Zn^{2+} Complexes in MeCN[a]

	free ligand		complex		
ligand	λ_{max}/nm	ε (L/mol/cm)	λ_{max}/nm	ε (L/mol/cm)	$\Delta\nu_{abs}$/cm^{-1}
1	335	50500	356	41920	1761
2	337	48766	357	42652	1662
3	334	55055	355	44414	1771
4	345	34285	374	28642	2248
5	348	43300	375	36050	2069
6	372	36835	417	30867	2901
7	383	33600	434	32700	3068
8	349	16181	345	12681	−332
9	343	50996	354	52804	906
11	373	35404	416	35548	2771

[a]Zn^{2+}-induced absorption band shifts ($\Delta\nu_{abs}$/cm^{-1}) are shown in the rightmost column.

Absorption Titration Studies. As supported by the computational studies (Table 1), increasing the electron density of the aryl group in AVMB leads to the enhanced

charge-transfer character of the Franck−Condon S$_1$ excited state, which results in bathochromic shifts of the absorption spectra (Table 3). Long absorption wavelengths are desired in zinc sensing applications, especially when live cellular samples are used, because autofluorescence-causing and physiologically damaging UV excitation can be avoided. On the other hand, the absorption spectra of all compounds but **8** undergo bathochromic shifts upon Zn^{2+}-coordination (e.g., spectra of **4** in Figure 7), which strengthens the elec-tron-accepting ability of the pyridyl group. The extent of the shift ($\Delta\nu_{abs}$/cm^{-1}) represents the stabilization of the Franck−Condon S$_1$ state of the AVMB by the Zn^{2+} ion at the negative end of its dipole moment. The more electron-donating aryl group (Ar in Figure 1B) results in a larger $\Delta\nu_{abs}$ value, due to a more favorable electrostatic interaction between Zn^{2+} and the negative end of a more polarized excited state dipole. Compound **8**, which has a strongly electron-withdrawing 4-nitrophenyl cap, undergoes a hyp-sochromic shift instead upon Zn^{2+} coordination, which corroborates the prior computed results (Table 1) that electron density of **8** shifts from the bipy side to the aryl side upon excitation.

In the compounds featuring weakly electron-donating (**1**, **2**, **3**) or weakly electron-withdrawing (**9**) groups, the molar absorptivities of the lowest energy bands in free ligands are high ($\sim$50 000). As stronger electron-donating groups are incorporated (**4**, **5**, **6**, **7**, **11**), the molar absorptivities drop to $\sim$30 000. Similar reduction in molar absorptivity of an AVMB was observed upon Zn^{2+}-coordination (**9** and **11** are the exceptions). The reduced molar absorptivities at wavelengths of maximum absorption as stronger electron-donating groups are incorporated and/or Zn^{2+} is bound (which enhances electron-accepting ability of the pyridyl) may be ascribed to the increasing degree of charge-transfer character of the transition. The small overlap density of the two molecular orbitals involved in a charge-transfer transition leads to a small transition moment, when results in a low probability of transition (eq 6).[59]

Fluorescence Titration Studies. The emission bands of most AVMBs (except **8**) also undergo bathochromic shifts upon Zn^{2+} binding (see spectra of **4** in Figure 7B). Increasing

(53) Bilyk, A.; Harding, M. M.; Turner, P.; Hambley, T. W. *J. Chem. Soc., Dalton Trans.* **1994**, 2783–2790.

(54) Murphy, B.; Aljabri, M.; Light, M.; Hursthouse, M. B. *J. Chem. Cryst.* **2003**, *33*, 195–202.

(55) Lemoine, P.; Bendada, K.; Viossat, B. *Acta Crystallogr.* **2004**, *C60*, m489–m491.

(56) Juric, M. S.; Planinic, P.; Giester, G. *Acta Crystallogr.* **2006**, *E62*, m2826–m2829.

(57) Kozhevnikov, D. N.; Shabunina, O. V.; Kopchuk, D. S.; Slepukhin, P. A.; Kozhevnikov, V. N. *Tetrahedron Lett.* **2006**, *47*, 7025–7029.

(58) Kozhevnikov, V. N.; Shabunina, O. V.; Kopchuk, D. S.; Ustinova, M. M.; König, B.; Kozhevnikov, D. N. *Tetrahedron* **2008**, *64*, 8963–8973.

(59) Montalti, M.; Credi, A.; Prodi, L.; Gandolfi, M. T. In *Handbooks of Photochemistry*; 3rd ed.; CRC Taylor and Francis: London, 2006; pp 28−30.

TABLE 4. Positions (λ_{max}) of the Lowest Energy Emission Bands and Stokes Shifts (SS) of Both Free Ligands and Their Zn^{2+} Complexes in MeCN[a]

	ligand		complex		
ligand	λ_{max}/nm	SS/cm^{-1}	λ_{max}/nm	SS/cm^{-1}	$\Delta\nu_{em}$/cm^{-1}
1	392	4341	459	6303	3724
2	392	4163	455	6033	3532
3	391	4365	460	6430	3836
4	431	5784	533	7976	4440
5	422	5039	504	6825	3855
6	480	6048	604	7425	4277
7	532	7313	712	8997	4752
8	551	10504	493	8702	−2135
9	403	4341	419	4382	948
11	480	5976	600	7372	4167

[a] Zn^{2+}-induced emission band shifts ($\Delta\nu_{em}$/cm^{-1}) are shown in the rightmost column.

electron density in the aryl moiety leads to a larger Zn^{2+}-induced shift ($\Delta\nu_{em}$, Table 4). The extent of shift ($\Delta\nu_{em}$) represents the combined effect of Franck−Condon excited state stabilization by Zn^{2+} coordination ($\Delta\nu_{abs}$) *and* differential solvent relaxation, which is the difference between the Stokes shifts of free ligand and Zn^{2+} complex (ΔSS, eq 7). The Stokes shifts of the complexes are larger than those of their respective free ligands (except **8** and **11**), indicating that the Franck−Condon excited state of the complex is more polar than that of the free ligand. On the other hand, the emission of the Zn^{2+} complex is less solvent-sensitive than that of the free ligand (Table 2), which suggests that the primary stabilization effect of the emissive S_1 state is resulted from the presence of Zn^{2+} rather than solvent reorganization (limited solubilities of the complexes in hexanes, benzene, and toluene prevented the collection of the emission spectra of in these solvents).

$$\Delta\nu_{em} = \Delta\nu_{abs} + \Delta SS \qquad (7)$$

$\Delta\nu_{em}$ and $\Delta\nu_{abs}$, emission and absorption band shifts upon Zn^{2+} coordination, respectively, in wavenumbers; ΔSS, the difference between Stokes shifts of the Zn^{2+} complex and the free ligand.

The structural dependence of the emission band shifts ($\Delta\nu_{em}$) and the fluorescence quantum yield changes (Table 5) upon zinc binding provides a foundation for developing ratiometric indicators for zinc effective within various emission windows. On the other hand, the correlation between the electron density of the aryl group and the Zn^{2+}-effected emission band shift potentially poses a dilemma in fluorescent heteroditopic ligand design for achieving high contrast between three fluorescence states shown in Figure 1A. An electron-rich aryl group would lead to a large Zn^{2+}-effected emission shift which results in a large contrast between the mono- and dizinc complexes. However, increasing electron density in the aryl group would also increase the oxidation potential of the AVMB ligand which attenuates the CHEF effect, thus reducing the contrast between the fluorescence of the free and monozinc-bound ligands. This dilemma will be examined and addressed in a future study.

Lifetime and Fluorescence Quantum Yields of Ligands and Zn^{2+} Complexes. The fluorescence quantum yield change upon Zn^{2+} coordination in MeCN (Table 5) does not follow a simple correlation with the electronic nature of

the aryl group. In order to gain more insight in the change of excited state decay processes upon Zn^{2+} coordination, lifetimes of both AVMB ligands and their Zn^{2+} complexes were measured and the rate constants of radiative and nonradiative decays were calculated (Table 5). Lifetime values generally increase upon Zn^{2+} complex formation. The ligands that show charge-transfer characters (**1**−**6**, **11**) have lifetimes of their Zn^{2+} complexes ≥2 ns. For **8** and **9** that do not exhibit a charge-transfer character, the lifetimes of Zn^{2+} complexes are shorter (1.20 and 1.60 ns, respectively). Both k_r and k_{nr} of a ligand drop upon Zn^{2+} coordination. The reduction of k_r upon Zn^{2+} binding can be explained using eq 5. The decrease in k_{nr}, on the other hand, may be partly due to the reduction of rotational freedom upon Zn^{2+} binding. The rigidifications of Haley's cross-conjugated phenylacetylenes[5] and Finney's biphenyls[60] and biarylacetylenes[61] were shown to enhance fluorescence quantum yields over their unlocked precursors, presumably via reducing k_{nr}. As both k_r and k_{nr} decrease upon Zn^{2+} binding, the collective effect which contributes to the change in fluorescence quantum yields does not have a simple correlation with the electronic nature of the aryl group. Some interesting observations are described in the next paragraph.

Compounds **1**−**3** contain electronically neutral (or weakly donating) aryl groups. The fluorescence quantum yields of **1**−**3** in MeCN are high (0.6−0.8) in both free ligands and complexes. The emission band shifts upon Zn^{2+} coordination are moderate (3500−3800 cm^{-1}). For compounds **4** and **5** with electron-donating groups of intermediate strengths, the fluorescence quantum yields undergo significant enhancement upon Zn^{2+} binding. The emission band shifts are larger than those of **1-3**. For compounds featuring even stronger electron-donating groups (**6**, **7**, **11**), large emission band shifts (>4000 cm^{-1}) were also observed. However, their fluorescence quantum yields either remain unchanged or decrease upon Zn^{2+} coordination. In the case of **7**, highly efficient fluorescence quenching was observed upon binding Zn^{2+} in MeCN. A similar observation was reported by Tor et al. where 3,8-di(4-dimethylaminophenylethynyl)-1,10-phenanthroline underwent fluorescence quenching upon Zn^{2+} complex formation in MeCN.[15] For compounds **8**−**9** containing electron-withdrawing groups, the emission band shifts are much smaller. The S_1 excited states of nitro-containing compounds are often resulted from the n−π* transitions,[62] which might explain the low ϕ_f's of **8** and its complex. On the other hand, compound **9** featuring a much weaker electron-withdrawing cyano group undergoes a noticeable fluorescence enhancement upon Zn^{2+} coordination.

More intricacies in the fluorescence properties of different species during Zn^{2+} titration experiments were revealed by the titration isotherms. For example, the absorption spectrum of compound **6** undergoes a bathochromic shift upon $Zn(ClO_4)_2$ addition in MeCN with an apparent isosbestic point at 395 nm (Figure 8A). The binding isotherm (Figure 8B) suggested a 2:1 (ligand to Zn^{2+}) or 3:1 complexation. The fluorescence titration, on the other hand,

(60) McFarland, S. A.; Finney, N. S. *J. Am. Chem. Soc.* **2001**, *123*, 1260–1261.
(61) McFarland, S. A.; Finney, N. S. *J. Am. Chem. Soc.* **2002**, *124*, 1178–1179.
(62) Suppan, P.; Ghoneim, N. In *Solvatochromism*; The Royal Society of Chemistry: London, 1997; pp 105.

TABLE 5. Fluorescence Quantum Yields (ϕ_f), Lifetime (τ),[a] and Rates of Radiative (k_r) and Nonradiative (k_{nr}) Decays of Ligands and Their Zn^{2+} Complexes in MeCN

	ligand					complex				
	τ/ns	χ^2	ϕ_f	k_r/ns^{-1}	k_{nr}/ns^{-1}	τ/ns	χ^2	ϕ_{Zn}	k_r/ns^{-1}	k_{nr}/ns^{-1}
1	1.06	1.31	0.67	0.63	0.31	2.41	1.19	0.77	0.32	0.10
2	1.01	0.73	0.76	0.75	0.24	2.14	0.64	0.82	0.38	0.08
3	0.99	0.50	0.69	0.70	0.31	2.30	0.52	0.79	0.34	0.09
4	0.58	0.57	0.28	0.48	1.24	3.14	1.28	0.46	0.15	0.17
5	0.23	0.64	0.042	0.18	4.17	1.91	1.30	0.25	0.13	0.39
6	0.51	0.47	0.087	0.17	1.79	2.76	0.78	0.10	0.04	0.33
7	1.22	1.02	0.34	0.28	0.54	ND^b	ND^b	0.0002	ND^b	ND^b
8	0.31	0.99	0.045	0.15	3.08	1.20	0.93	0.019	0.02	0.82
9	0.60	0.94	0.27	0.45	1.22	1.60	0.41	0.65	0.41	0.22
11	0.66	1.30	0.13	0.20	1.32	2.91	1.77	0.13	0.04	0.30

[a]In the TCSPC experiments, all samples were excited using a 370 nm LED. The fluorescence decays were observed at the respective emission λ_{max} shown in Table 4. [b]ND, Not Determined due to very low fluorescence quantum yield of the Zn^{2+} complex of **7**.
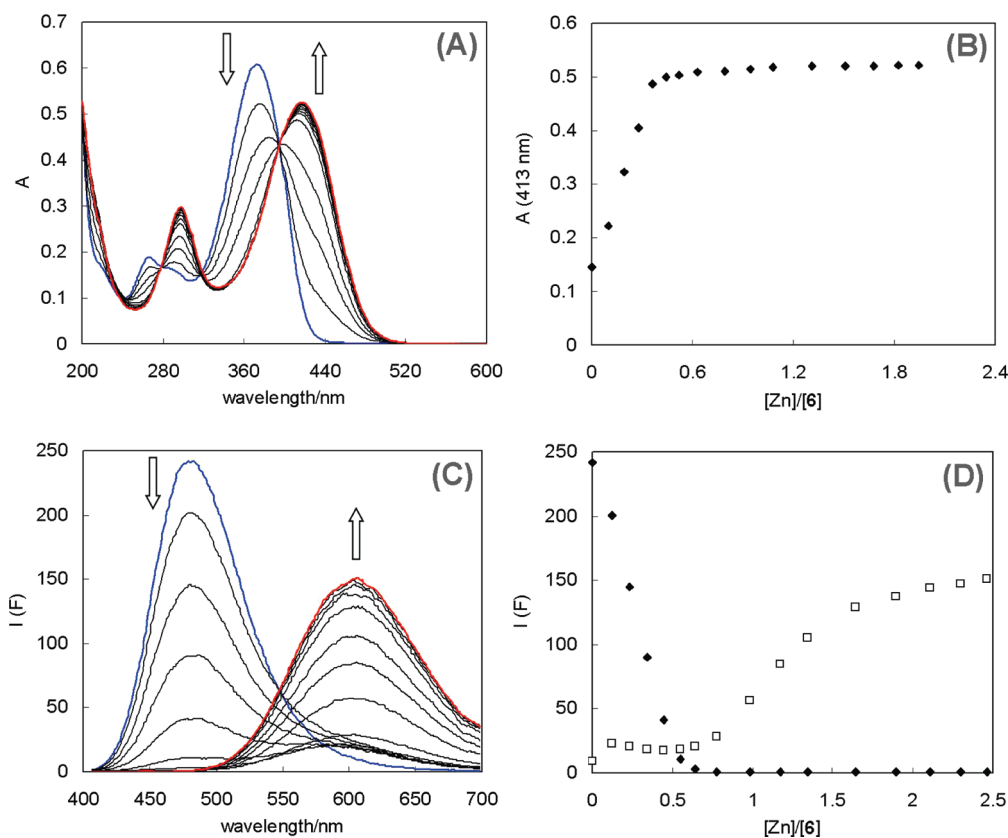
FIGURE 8. (A) Spectrophotometric titration of **6** (17 μM) with $Zn(ClO_4)_2$ (0 − 34 μM) in MeCN. Blue spectrum, [Zn(II)] = 0; red spectrum, [Zn(II)] = 34 μM. Arrows show the spectral change upon Zn^{2+} addition. (B) Absorbance of **6** (17 μM) at 413 nm vs [Zn(II)]/[L]. (C) Fluorescence titration of **6** (5.3 μM, λ_{ex} = 397 nm) with $Zn(ClO_4)_2$ (0−13 μM) in MeCN at 25 °C. Blue spectrum, [Zn(II)] = 0; red spectrum, [Zn(II)] = 13 μM. Arrows show the spectral change upon Zn^{2+} addition. (D) Fluorescence intensity of **6** (5.3 μM) at 483 nm (♦) and 607 nm (□) vs [Zn(II)]/[L].

produced much richer information. Overall, with addition of Zn^{2+} the fluorescence at 483 nm decreases and the band at 607 nm increases (Figure 8C). However, the fluorescence attenuation at 483 nm and enhancement at 607 nm, that is, the emission "bathochromic shift", are not synchronized during the entire titration process. Three transitions were identified in the emission isotherm (Figure 8D). At the very earliest stage, the "bathochromic shift" is synchronized[63] followed by a period during which the monotonous reduction

of the free ligand emission was observed. As the fluorescence of the free ligand all but disappears, the emission at 607 nm starts to increase. Clearly, the enhancement at 607 nm during the third leg of the titration is not due to the conversion of the free ligand to the Zn^{2+} complex because the free ligand has already been consumed judged by the disappearance of the band at 483 nm. The current hypothesis, corroborated by the ITC study, is that the Zn^{2+} titration first affords weakly emissive 3:1 and 2:1 (ligand to Zn^{2+}) complexes. The fluorescence quenching observed at this stage may be attributed to the interfluorophore interactions in the 3:1 or 2:1 complexes. When all the free

---

(63) See Figure S25, SI, for data collected from another independently prepared sample.

ligands are consumed, further addition of Zn^{2+} converts the 3:1 or 2:1 complex to the much more emissive 1:1 complex (The absorption spectra of all the Zn^{2+} complexes with different association stoichiometries, however, are similar in this hypothesis). Therefore, the delayed fluorescence enhancement at 607 nm was observed. The unsynchronized emission "bathochromic shifts" are not unique to compound **6**. All ligands investigated in this study display this behavior to various degrees.

Conclusion

The photophysical properties and Zn^{2+} coordination chemistry in MeCN of fluorescent 5-arylvinyl-5′-methyl-2,2′-bipyridyl (AVMB) ligands are described. The primary objective is to reveal the factors that control the emission band shift and fluorescence quantum yield change of the AVMB ligands upon Zn^{2+} coordination. The solvent dependency studies and computational analysis of free ligands support the charge-transfer nature of the S_1 excited states of most ligands, as we have invoked in previous studies.[34,35] The Zn^{2+} coordination in MeCN was investigated by, in addition to spectroscopic means, isothermal titration calorimetry (ITC). A multiple species equilibrium involving the formation of 3:1 and/or 2:1 (ligand to Zn^{2+}) complexes en route to the eventual 1:1 complex best explains the observed ITC traces in which $Zn(ClO_4)_2$ was used as the Zn^{2+} source. When $ZnCl_2$ was used in the ITC experiment, a 1:1 stoichiometry was observed instead, demonstrating the counterion-dependence of binding stoichiometry.

The electron-donating ability of the aryl group is a major determinant of the magnitude of absorption and emission band shifts of an AVMB ligand upon Zn^{2+} coordination in MeCN. The coordination of Zn^{2+} at the negative end of the excited dipole greatly attenuates the energy of the excited state, leading to a bathochromic shift. The fluorescence quantum yield change, however, does not carry a similar correlation with the electronic nature of the aryl group. The Zn^{2+} coordination was found to reduce both radiative (k_r) and nonradiative (k_{nr}) decay rates, which collectively contribute to the change in fluorescence quantum yields. The decrease of k_r can be explained using eq 5 where k_r is proportional to the square of transition energy. The drop in k_{nr} may be attributed, in part, to the reduced degrees of rotational freedom of the molecule upon Zn^{2+} coordination. This study in the fundamental coordination chemistry and photophysics of the AVMB ligands, which is garnering increasing attention as the molecular optical components in various applications, is expected to aid the rational design of molecular sensors and possibly materials for energy conversion.

Experimental Section

Representative Procedures. Compound 2. NaH (160 mg, 60% in mineral oil, 4 mmol) was added at 0 °C to a solution of 4-chlorobenzaldehyde (39 mg, 0.28 mmol) in dry dimethoxyethane (4.0 mL) in a flame-dried round-bottom flask. The suspension was stirred for 5 min. A solution of **10** (90 mg, 0.28 mmol) in dry dimethoxyethane (4.0 mL) was added dropwise to the flask with stirring at 0 °C. The stirring was continued for overnight at rt. The reaction mixture was then cooled to 0 °C

before brine (2 mL) was added. The reaction mixture was stirred for another 5 min, and was partitioned between EtOAc and water. The aqueous layer was washed with EtOAc (50 mL × 3) and the organic portions were combined. The organic portions were dried over Na_2SO_4 followed by solvent removal under vacuum. Compound **2** was isolated using silica column chromatography eluted by EtOAc in DCM (gradient 0−30%). The isolated yield was 70% (54 mg). ^{1}H NMR (300 MHz, CDCl$_3$): δ/ppm 8.74 (s, 1H), 8.52 (s, 1H), 8.36 (d, J = 8.2 Hz, 1H), 8.30 (d, J = 8.2 Hz, 1H), 7.96 (dd, J = 2.4, 8.6 Hz, 1H), 7.64 (dd, J = 2.1, 8.1 Hz, 1H), 7.48 (d, J = 8.6 Hz, 2H), 7.36 (d, J = 8.5 Hz, 2H), 7.18 (d, J = 16.2 Hz, 1H), 7.10 (d, J = 16.5 Hz, 1H), 2.40 (s, 3H); ^{13}C NMR (75 MHz, CDCl$_3$): δ/ppm 155.6, 152.5, 149.9, 148.3, 137.7, 137.6, 135.5, 134.1, 133.6, 132.6, 129.6, 129.2, 128.1, 125.7, 120.9, 120.8, 18.6; HRMS (ESI+): calcd. ($C_{19}H_{15}ClN_2$+H$^+$) 307.1002, found 307.1005.

Compound 3. Compound **10** (102 mg, 0.32 mmol) was dissolved in anhydrous THF. t-BuOK (82 mg, 0.72 mmol) and 4-fluorobenzaldehyde (90 mg, 0.72 mmol) was added subsequently. The reaction mixture was allowed to stir for overnight after which the reaction was quenched carefully with water and extracted by EtOAc. The aqueous layer was washed with EtOAc (50 mL × 3). The combined organic layers were dried over Na_2SO_4 and the solvent was removed under reduced pressure. Compound **3** was isolated using silica column chromatography using EtOAc in DCM (0−30%). The isolated yield was 80% (71 mg). ^{1}H NMR (300 MHz, CDCl$_3$) δ/ppm 8.73 (d, J = 2.1 Hz, 1H), 8.50 (s, 1H), 8.35 (d, J = 8.3 Hz, 1H), 8.28 (d, J = 8.1 Hz, 1H), 7.93 (dd, J = 2.3, 8.1 Hz, 1H), 7.61 (dd, J = 1.6, 8.1 Hz, 1H), 7.50 (dd, J = 5.4, 8.7 Hz, 2H), 7.16 (d, J = 16.4 Hz, 1H), 7.04 (m, 3H), 2.38 (s, 3H); ^{13}C NMR (75 MHz, CDCl$_3$): δ/ppm 164.5, 161.2, 155.4, 153.5, 149.8, 148.1, 137.6, 133.5, 133.2, 132.7, 129.6, 128.5, 124.8, 120.7, 116.1, 115.8, 18.6; HRMS (ESI+): calcd ($C_{19}H_{15}FN_2$+H$^+$) 291.1298, found 291.1302.

Compound 11. Compound **6** (73 mg, 0.26 mmol) was dissolved in dry DCM (2.6 mL) in a round-bottom flask containing a magnetic stirr bar. The solution was cooled in an ice bath. A solution of Br_2 (13 μL, 0.26 mmol) in DCM (1.3 mL) was added dropwise to the reaction mixture through an addition funnel. After the addition, the stirring was continued for 2 h while the temperature was allowed to rise to rt. The solvent was carefully removed on a rotary evaporator with an aqueous $Na_2S_2O_3$ solution ($\sim$ 10 mL, 1 M) in the reservoir to absorb the residual Br_2. The crude product was partitioned between EtOAc (50 mL) and brine. After separation, the brine layer was washed with EtOAc (50 mL × 2) before all the organic fractions were combined and dried over anhydrous Na_2SO_4. TLC (silica plate, eluted with EtOAc) showed a light yellow spot which was later verified as the product. Compound **11** was purified on a silica column (eluted with 0−10% EtOAc in DCM). The yield was 48% (45 mg). ^{1}H NMR (300 MHz, CDCl$_3$): δ/ppm 8.68 (s, 1H), 8.51 (s, 1H), 8.33 (d, J = 8.4 Hz, 1H), 8.31 (d, J = 7.5 Hz, 1H), 7.91 (d, J = 2.4 Hz, 1H), 7.63 (d, J = 6.6 Hz, 1H), 7.05 (d, J = 16.2 Hz, 1H), 6.87 (d, J = 16.2 Hz, 1H), 6.55 (d, J = 3.6 Hz, 1H), 6.24 (d, J = 4.2 Hz, 1H), 3.69 (s, 3H), 2.41 (s, 3H); ^{13}C NMR (75 MHz, CDCl$_3$): δ/ppm 154.8, 153.5, 149.8, 147.7, 137.6, 133.4, 133.1, 132.9, 132.8, 122.4, 120.7, 120.6, 119.1, 111.5, 108.1, 105.0, 32.6, 18.5; HRMS (ESI+): calcd. ($C_{18}H_{16}BrN_3$+H$^+$) 354.0558, found 354.0578.

Supporting Information Available: Synthetic procedures and characterization of new compounds, additional spectra, fluorescence decay traces, and cyclic voltammograms. This material is available free of charge via the Internet at http://pubs.acs.org.